Biosensors and Bioelectronics ■ (■■■■) ■■■–■■■

Contents lists available at ScienceDirect

Biosensors and Bioelectronics

journal homepage: www.elsevier.com/locate/bios

Parylene-based flexible neural probes with PEDOT coated surface for brain stimulation and recording

V. Castagnola [a,b,*], E. Descamps [a,b], A. Lecestre [a,b], L. Dahan [c], J. Remaud [c], L.G. Nowak [d], C. Bergaud [a,b]

[a] CNRS, LAAS, 7 avenue du colonel Roche, F-31400 Toulouse, France
[b] University of Toulouse, LAAS, F-31400 Toulouse, France
[c] Centre de Recherche sur la Cognition Animale (CRCA), University of Toulouse, France
[d] Centre de Recherche Cerveau et Cognition (CerCo), CNRS, Toulouse, France

ARTICLE INFO

Article history:
Received 5 June 2014
Received in revised form
14 August 2014
Accepted 2 September 2014

Keywords:
Parylene
Neural probes
PEDOT
Flexible

ABSTRACT

Implantable neural prosthetics devices offer a promising opportunity for the restoration of lost functions in patients affected by brain or spinal cord injury, by providing the brain with a non-muscular channel able to link machines to the nervous system. Nevertheless current neural microelectrodes suffer from high initial impedance and low charge-transfer capacity because of their small-feature geometry (Abidian et al., 2010; Cui and Zhou, 2007). In this work we have developed PEDOT-modified neural probes based on flexible substrate capable to answer to the three critical requirements for neuroprosthetic device: efficiency, lifetime and biocompatibility. We propose a simple procedure for the fabrication of neural electrodes fully made of Parylene-C, followed by an electropolymerization of the active area with the conductive polymer PEDOT that is shown to greatly enhance the electrical performances of the device. In addition, the biocompatibility and the very high SNR exhibited during signal recording make our device suitable for long-term implantation.

1. Introduction

Many different disorders can disrupt the communication of the brain with the external environment. Neuroprosthetics may offer the possibility to restore sensory or motor functions by providing the brain with an external communication and control channel, as in the Brain Computer Interface (BCI). Moreover neural probes are employed for the treatment of numerous diseases such as Parkinson's disease, dystonia and chronic pain (Hochberg et al., 2006; Schwartz et al., 2006). The implantation of neural interfaces for long periods of time has rapidly becoming an invaluable clinical and diagnostic tool (Kipke et al., 2008). Although neural electrodes have been successfully used and demonstrated clinical relevance (deep brain stimulation, cochlear implants) some issues remain to be addressed. In particular, the efficiency, the biocompatibility and the stability of the implanted electrodes are far from being optimized; in many cases, penetrating recording electrodes fail within weeks or months (Griffith and Humphrey, 2006) because the recording capability usually deteriorates over time. This lack of long-term reliability must be improved to make these technologies viable for widespread use (Polikov et al., 2005). The degradation of signal quality in chronically implanted microelectrodes is attributed to both biotic factors, such as the hypothesis that the glial scar, constituted primarily by astrocytes and microglia, encapsulates the electrodes (Kotov et al., 2009), functionally insulating the recording surfaces, and to abiotic factors, such as insulation delamination, corrosion and strain due to micromotions (Streit et al., 2012; Biran et al., 2007). Another reason for electrode failure can be breakage of electrode leads caused by mechanical stress. Moreover, a common hypothesis is that micromotions or rather microforces between the implanted probe and the tissue cause small injuries that constantly maintain an inflammatory process (Polikov et al., 2005). Histological studies (Biran et al., 2007; Kim et al., 2004) report that the strain induced immune response, caused by the rigid tethering of the electrode to the skull, leads to an increase in microglial activity in the implanted tissue as compared to untethered electrodes (Gilletti and Muthuswamy, 2006). Quantitative studies have shown that electrode with low Young's modulus material or redefined geometry for high compliance can provide front-end strain relief and polymers such as polyimide and Parylene-C, with their good biocompatibility, have been the choice of researchers for electrode substrate materials(Sankar et al., 2013; Seymour et al., 2011; Ziegler

* Corresponding author at: CNRS, LAAS, 7 avenue du colonel Roche, F-31400 Toulouse, France.
E-mail addresses: vcastagn@laas.fr (V. Castagnola), edescamp@laas.fr (E. Descamps), alecestr@laas.fr (A. Lecestre), lionel.dahan@univ-tlse3.fr (L. Dahan), jessica.remaud@univ-tlse3.fr (J. Remaud), lionel.nowak@cerco.ups-tlse.fr (L.G. Nowak), bergaud@laas.fr (C. Bergaud).

http://dx.doi.org/10.1016/j.bios.2014.09.004
0956-5663/

et al., 2006; Kim, 2013; Rodger et al., 2008; Metallo et al., 2011). Furthermore it is well known that the miniaturization of the electrode size is a critical requirement for single neuron recording and for electrical stimulation restricted to small populations of neuronal elements. In fact, a single square millimeter of brain tissue contains approximately one million neurons. To match this number and density, future BMIs must feature smaller and denser electrode arrays in order to precisely monitor and control neural circuit activity. Unfortunately a significant reduction in electrode size greatly increases electrode impedance, limiting the recording sensitivity and the maximum stimulating current deliverable through the electrode–tissue interface. Chronic implantable microelectrodes should exhibit low impedance for recording or safe charge injection for stimulation to ensure a good quality of bidirectional communication with the neural tissue. In order to address these issues, a reduction in electrode size should not be done at the expense of electrode function and the interface, where the physical contact between the brain and the neuroprosthesis occurs, is then the key element of the device.

Conductive polymers, serving as stable electron- and ion-conducting biomaterials, are widely used as interfaces with nerve cells for recording their activities (Abidian et al., 2010; Asplund et al., 2010; Harris et al., 2013). Among conductive polymers, poly(3,4-ethylenedioxythiophene) (PEDOT) has been the subject of much interest because of its well-known properties such as high-conductivity, biocompatibility, excellent stability and transparency in its doped state (Aregueta-Robles et al., 2014). Yamato et al. (1995) reported that PEDOT:PSS was more chemically stable than PPy:PSS (Polypyrrole).

In this work we propose a simple fabrication procedure for neural probes fully made of Parylene-C in which, for the first time on a highly flexible multielectrode device, the active electrode area is electrochemically modified with PEDOT, in order to enhance the electrical properties and the stability at the electrode–tissue interface. By combining the capability of Parylene-C to conform to living tissue with the modification of the electrode interface, we propose an answer to the major critical requirements for long-term implantation of a neural probe.

2. Experimental

2.1. Materials

The Parylene C (PXC) dimer was provided by Comelec SA. Both the 3,4-ethylene dioxythiophene (EDOT) and the Poly (sodium 4-styrenesulfonate) (NaPSS, average Mw=70,000) were provided by Sigma Aldrich and used as received. Deionized water was used to prepare all solutions. Dulbecco's Modified Eagle Media (D-MEM), Horse Serum (Heat Inactivated), Fetal Bovine Serum, Antibiotic–Antimycotic (containing penicillin–streptomycin), and Trypsin were purchased from Thermo Scientific (HyClone). SH-SY5Y cell line was kindly provided by the Institut de Pharmacologie et de Biologie Structurale (IPBS) of Toulouse. The LIVE/DEAD Viability/Cytotoxicity Kit for mammalian cells was purchased from Invitrogen.

2.2. Fabrication of Parylene-based neural probes

The implantable microelectrodes fabrication process is schematized in Fig. 1.

A standard 4 p-type silicon wafer of (100) orientation with a thickness of 525 μm was used as a substrate for the whole process. Parylene-C (Fig. 1a) was deposited through thermally activated CVD machine C30S, provided by Comelec SA at the pyrolysis temperature of 700 °C. The thickness of the deposition, measured each time by standard Profilometer (KLA Tencor), is directly related to the mass of precursor dimer loaded in the sublimation chamber. A 23 μm-thick PXC (Parylene-C) film was obtained starting from 80 g of precursor. It will constitute the substrate of the final device.

Gold (Au) circular electrodes were patterned on the PXC surface thanks to a metallization followed by a lift-off process. First, a negative photoresist (AZ-nLOF 2035, MicroChemicals) was patterned on the wafer (Fig. 1b), using a Mask Aligner MA150 (Karl Suss), then a 200 nm-thick Au layer was evaporated on the wafer (a 50 nm-thick Ti layer, also obtained by evaporation, was used to improve adhesion between PXC surface and Au). The electron beam physical vapour deposition was performed using the equipment EVA 600 (Alliance Concept) at room temperature (20 ± 1 °C) at a working pressure of 2×10^{-7} mbar, leading to a deposition rate of 1 nm/s both for Au and Ti. A lift-off process was performed after the Ti/Au evaporation by dipping the wafer in an acetone bath overnight (Fig. 1c). After the Au electrode patterning, a thin layer of PXC (about 800 nm obtained from 1.6 g of precursor) is deposited on top of the wafer as a passivation layer (Fig. 1d). The electrode surfaces and the contacts were opened by dry etching of the PXC using a photoresist mask (AZ-ECI 3027, MicroChemicals) with a thickness of about 2 μm (Fig. 1e). The plasma etching has been performed using a Plasma equipment RIE-ICP (Trikon Omega 201). The etching parameters have been optimized as follows: T=10 °C, O_2=20 sccm; P_r=20 mT; P_{ICP}=500 W; P_{bias}=10 W. The etching rate of PCX with these parameters was found to be

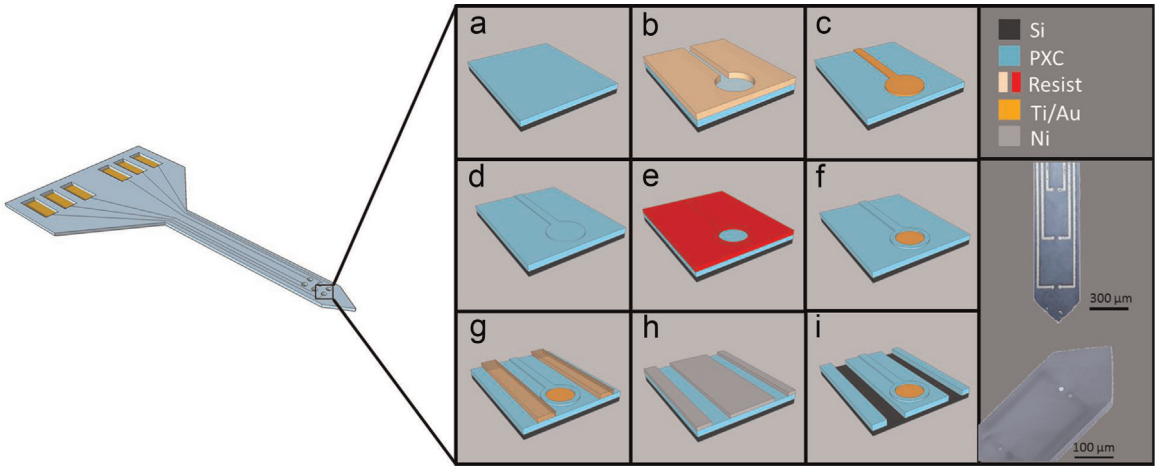

Fig. 1. Schematic illustration of the main steps to fabricate the Parylene-based microelectrodes.

Please cite this article as: Castagnola, V., et al., Biosensors and Bioelectronics (2014), http://dx.doi.org/10.1016/j.bios.2014.09.004

350 nm/min, where the etching rate of AZ-ECI photoresist is about 450 nm/min (Fig. 1f). The wafer surface was previously patterned with AZ-nLOF 2035 photoresist (Fig. 1g), then a layer of 100 nm of Nickel (Ni) was deposited by electron beam physical vapour deposition on top of it, at a working pressure of 2×10^{-7} mbar, leading to a deposition rate of 0.2 nm/s, and a second lift-off procedure was performed in order to use the Ni layer as a hard mask for the second etching process (Fig. 1h). The plasma oxygen etching was performed as described above during a time duration (roughly up to 70 min) long enough to allow the cutting of the 24 μm-thick layer of PXC. The Ni layer was then chemically etched in a mixture of HCl (20%) and H_2O_2 (10%) in deionized water (Fig. 1i). Finally the PXC on the edge of the Si wafer was scratched with tweezers and the electrode structures were easily peeled-off from the Si surface, keeping their planar shape, without the use of any sacrificial layer.

2.3. Electrochemical polymerization

In a classical three-electrodes cell, 200 nm-thick circular gold electrodes with a diameter ranging from 10 μm to 50 μm were used as working electrodes, a platinum wire was used as the counter electrode and a standard calomel electrode (SCE) as the reference. The solutions were de-aerated by bubbling N_2 for 20 min prior to all electrochemical experiments, which were successively carried out under N_2 atmosphere. For the electropolymerization of PEDOT, monomer/electrolyte solutions at different concentrations were used as well as different parameters for the cyclic voltammetry (CV), depending on the electrode size. A range of solutions from PEDOT 0.1%/PSS 0.8% to PEDOT 0.25%/PSS 0.2% in deionized water was used as starting monomer solution for the electropolymerization. Different potentials ranging from −0.9 V to 1.1 V were used for the CV at scan rates between 0.05 and 0.01 V/s.

2.4. Characterization

Cyclic Voltammetry (CV) and Electrochemical Impedance spectroscopy (EIS) measurements were carried out using a VMP3 Biologic potentiostat coupled with EClab Software at room temperature (23 ± 1 °C). A solution of NaCl 0.9% was used as the electrolyte in the cell. The impedance spectra were recorded at fifty discrete frequencies, by applying 0.05 V RMS sine wave with frequencies varying logarithmically over a frequency range of 1–10^4 Hz. CV was performed with the same apparatus by voltage sweeping between 0.6 V and −0.6 V vs. SCE, with a scan rate of 0.05 V/s. All the Scanning Electron Microscopy images were performed with a SEM Hitachi S-4800 while all the optical microscope images were performed with a Hirox Microscope HI-SCOPE Advanced KH-3000. Cell observation after staining was carried out with a florescence microscope DMIRB (Leica), using a Lumencor (Optoprim) as light source. The fluorescence images were treated with the software ImageJ.

2.5. Cell culture

SH-SY5Y human neuroblastoma cell lines were cultured in Dulbecco's modified Eagles medium (DMEM) supplemented with 10% fetal bovine serum, 1% L-glutamine and 1% penicillin–streptomycin and passaged using a solution of 0.25% trypsin. Cells were maintained at 37 °C in a humid 5% CO_2 atmosphere and were passaged at least three times after defrosting before any test procedure was applied. For the LIVE/DEAD ® Viability/Cytotoxicity, SH-SY5Y cells were cultivated in Petri dishes and after 24 h, 72 h and 168 h, a solution of 2 μM calcein AM and 2M EthD-1 in PBS was added. Samples were incubated at 37 °C for 30 min light protected, then, after rinsing 2 times with PBS, the samples were observed at the fluorescence microscope. The fixation procedure for SEM observation was performed as follows: 1 ml of glutaraldehyde solution (4% in H_2O) was added for each sample, leaving them in the fridge overnight. The fixation was followed by a dehydratation procedure, achieved by a sequential adding of ethanol at different concentration in H_2O (25%, 50%, 70%, 90%, 100%). The sample was left 15 min in each ethanol solution then rinsed three times with PBS.

2.6. In vitro electrophysiological recordings

The protocol for *in vitro* brain slice preparation was adapted from Nowak and Bullier (1996) and is briefly summarized here. Adult (>2 month old) female mice were deeply anesthetized with isoflurane and killed by decapitation. The scalp, skull and dura mater where taken off and the brain was removed. These operations were made in the presence of ice-cold, modified artificial cerebrospinal fluid (ACSF composition in mM: NaCl – 124, $NaHCO_3$ – 26, KCl – 3.5, $MgSO_4$ – 1, $MgCl_2$ – 9, NaH_2PO_4 – 1.25, and glucose – 10). Brain slices (400 μm thick) were cut on a vibratome (752M vibroslice, Campden Instrument, UK). Once obtained, the slices were kept at room temperature for at least 1 h in a storage chamber filled with an *in vivo*-like artificial cerebrospinal fluid (ACSF, composition in mM: NaCl – 124, $NaHCO_3$ – 26, KCl – 3.5, $MgSO_4$ – 1, NaH_2PO_4 – 1.25, $CaCl_2$ – 1.2, and glucose – 10). The ACSF was aerated with a 95% O2–5% CO_2 mixture (pH 7.4). For recording, one slice was placed on the net of a submersion recording chamber (Scientific System Design, Mississauga, Ontario, Canada). The temperature was maintained at 33–34 °C. The ACSF was gravity fed at a flow rate of 2.5–3.5 ml/min. Extracellular recordings of spontaneously active neurons were performed in the hippocampus (CA1, CA3). Signals were amplified and filtered with a Neurolog recording system (gain $\times 10^3$ or $\times 10^4$), and digitized with a 1401plus interface (CED Systems, Cambridge, UK) with a digitization rate of 20–40 kHz. On-line visualization and off-line analysis were achieved using Spike2 (CED Systems) software.

2.7. In vivo electrophysiological recordings

Two male C57BL/6J mice (10–16 weeks old, obtained from Charles River) were deeply anaesthetized with vetoflurane (2%) and secured to a stereotaxic apparatus placed in a faraday cage. Lidocaine was applied before (subcutaneous) and after skin incision. A craniotomy was performed to allow unilateral access to the hippocampus. The Parylene hex-trode (scheme in Fig. 1 – Supplementary Information) was then lowered in the hippocampus (1.8 mm posterior, 1.3 lateral and 1.1 ventral to the Bregma) and a stainless steel screw was placed through the occipital bone to serve as a reference and ground electrode. Electrophysiological recordings were made using each electrode of the hex-trode. The signal was filtered and amplified (0.3 Hz–3 kHz; P511, Grass Instruments, West Warvick, USA) fed to a 50 Hz noise eliminator (Hum-Bug, Quest Scientific, Vancouver, Canada) before being digitalized at 10 kHz (1401Plus, CED Systems, Cambridge, UK) and visualized and analyzed using Spike2 software (CED Systems).

3. Results and discussion

3.1. Probe structure

Nowadays the most common commercially available implantable neural microprobes are silicon-based (Rousche and Normann, 1998); however, imperfect contact and poor conformity to the curved surface of target tissues have been reported during

the use of penetrating electrode arrays based on rigid substrate (Lind et al., 2013; Polikov et al., 2006). The use of a flexible substrate can reduce the risk of injury during and after implantation, when the electrode is subjected to the brain movements. Moreover it improves the mechanical compliance with the brain tissue and promotes an intimate contact between electrodes and neural cells. To that purpose, Parylene C (PXC) represents one of the most promising materials due to its adequate mechanical properties, high biocompatibility (ISO 10993, United States Pharmacopeia (USP) Class VI material) and stability in wet microfabrication processes.

3.2. Electrochemical polymerization of PEDOT on the electrode surface

The use of microelectrodes (in our case with a diameter ranging from 10 μm to 50 μm) minimizes the reactive cell response and provides high density of electrode sites but, as the electrode dimensions decrease, the impedance increases affecting the quality of signal recordings (Cui and Zhou, 2007). Signal transduction at the electrode/tissue interface is indeed a complex function of electrode properties and tissue characteristics. Transduction between the ionically conducting tissue and the electronically conducting electrode primarily takes place through capacitive and/or Faradaic currents from reversible reduction-oxidation reactions at the electrode surface.

Since the electrode/tissue interface plays a key role in this context, we modified the gold electrode surface with the conducting polymer Poly (3,4-ethylene) dioxythiophene (PEDOT) that has emerged as an interesting candidate for neuroelectronic interfaces thanks to its excellent conductivity, stability properties and its good compatibility with biological structures (Asplund et al., 2009; Xiao et al., 2006; Aregueta-Robles et al., 2014). Cui et al. (2001) established that electrochemical polymerization can be used to deposit coatings of electrically conducting polymers directly onto metal neural electrode sites; moreover this technique allows to obtain very homogeneous, stable and resistant depositions. Poly (styrene sulfonate) (PSS), that has been chosen as counterion for PEDOT, plays the role of supporting electrolyte, also providing a better dissolution of EDOT monomer in H_2O (Castagnola et al., 2014). The electropolymerization of PEDOT takes place through the oxidation of the monomer that leads to a radical coupling; when the oligomers chains are long enough, they precipitate onto the electrode, generating the first polymer nuclei. During this step the process is controlled by the diffusion of the monomers; later, different nuclei combine together forming polymer globules. In the nucleation stage, the expansion of the polymer chains and the growth of globules on the electrode surface are the prevailing processes and, when the oxidation potential is applied for a certain period, globules begin to overlap until a full coverage of the surface with polymer globules is reached. Based on several studies (Castagnola et al., 2014), the potentiodynamic route of polymerization has been chosen to get high homogeneity and good electrical performances. The polymerization parameters vary with the electrode size. For 10 μm-diameter electrodes a cyclic voltammetry was performed in a classical three-electrodes cell configuration by applying a potential scan from −0.7 V vs. to 1 V vs. SCN at a scan rate of 0.01 V/s. Deaeration was obtained by purging the solution with nitrogen during 20 min. The oxidation of the monomer starts at 0.75 V and the anodic current reaches a peak value at 0.9 V. In the reverse scan the current decreases with a crossover at about 0.7 V; this “nucleation loop” reveals the nucleation process of the polymer film. The voltammogram also reveals a quasi-reversible signal at a potential close to −0.4 V corresponding to the redox activity of the polymer (Sekli-Belaidi et al., 2010) (see Fig. 4 – Supplementary Information).

3.3. Morphology of the PEDOT deposition

Many parameters, such as temperature, monomer concentration, applied voltage, scan rate, etc., influence the resulting morphology of the PEDOT electrodeposition. For 10 μm-diameter electrodes, the use of lower concentrations of monomer, lower upper vertex potentials and lower scan rates leads to a more homogeneous deposition and better performances in terms of impedance properties (Fig. 2).

3.4. Probe electrical properties

Fig. 3 depicts Bode graphs of the impedance magnitude over a frequency range of 1–10^4 Hz, for a gold electrode of 10 μm in diameter, before and after polymerization of PEDOT:PSS. The impedances of the electrode at 1 kHz were used for comparison purposes as action potentials have a characteristic frequency band centred at that frequency. The mean impedance at 1 kHz for the unmodified gold electrodes was around 700 k Ω, while after PEDOT electrochemical deposition, the mean impedance fell to ca. 10 k Ω. A CV with a scan of potential between −0.6 V and 0.6 V, at a scan rate of 0.05 V/s, was performed for comparing the charge injection capacity between the uncoated gold electrodes and the PEDOT-modified electrodes. High charge capacity, which is the measurement of charge transfer efficiency, should greatly improve

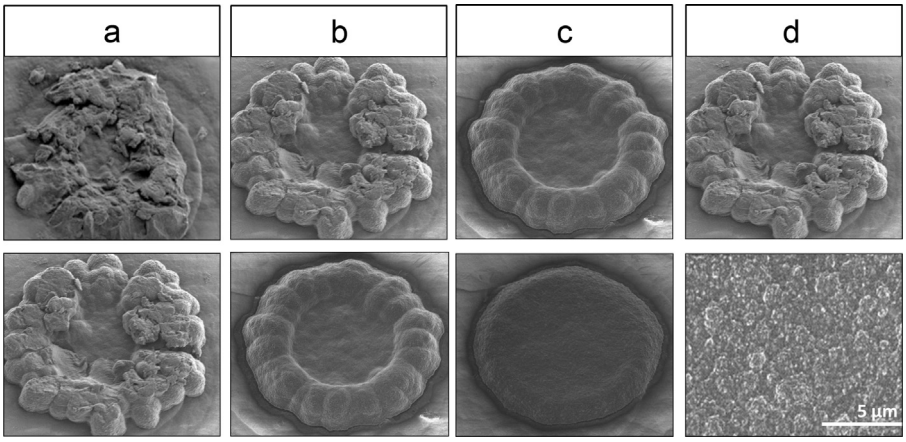

Fig. 2. SEM images of different morphologies of PEDOT:PSS layers related to different electrochemical deposition parameters: (a) 10 μm diameter electrode not cleaned (above) and cleaned (below) in H_2SO_4, (b) 0.1% of EDOT (above) and 0.025% of EDOT (below), (c) upper maximum potential at 1.1 V (above) and 1 V (below) and (d) 10 μm diameter electrode (above) and 50 μm diameter electrode (below).

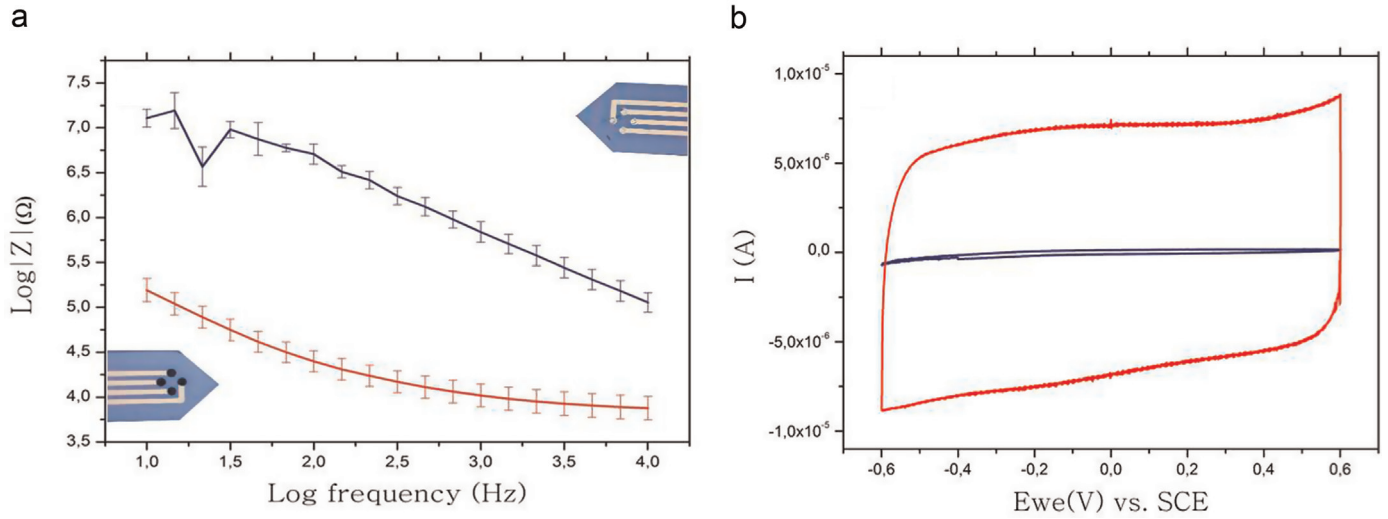

Fig. 3. (a) Electrochemical mean impedance spectroscopy over a range of 10–10^4 Hz and related error bar and (b) charge capacity for the pristine gold electrode (blue) and for the PEDOT-modified electrode (red) for a 10 μm diameter electrode in a NaCl 0.9% solution. (For interpretation of the references to color in this figure caption, the reader is referred to the web version of this article.)

recording of action potentials and stimulation of neuronal elements at a lower charge density at the device-tissue interface.

In the previous work (Castagnola et al., 2014) the electrical stability of this deposition, after thermal accelerated ageing precess, has been shown.

3.5. *In vitro biocompatibility assay*

The materials we used (PXC, PEDOT:PSS and gold) have been especially chosen for their properties of biocompatibility with living systems in order to design a device suitable for long-term implantation. PXC, as we mentioned in Section 3.1, has a certified biocompatibility of CLASS VI, and the cytotoxicity of PEDOT:PSS (Asplund et al., 2009; Richardson-Burns et al., 2007a) and gold (Zitter and Plenk, 1987; Edelman et al., 2001) have been investigated in the literature. For example, Asplund et al. (2009) indicate a non-cytotoxic of PEDOT:heparin surfaces and show no marked difference in immunological response in cortical tissue compared to pure platinum controls. Through cell viability assay, we set the preliminary objective to establish the non-cytotoxicity of the produced devices, after the clean room process, and further investigations on biocompatibility are scheduled in the near future. Therefore, we first carried out *in vitro* experiments to ensure that any armful chemical product remains on the wafer after the fabrication process and the electropolymerization.

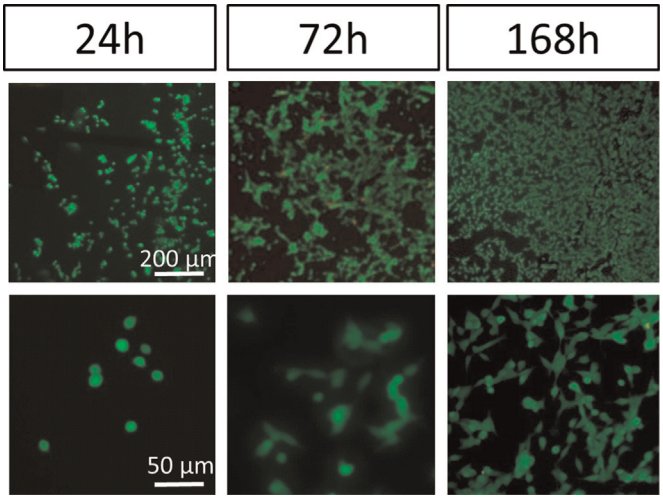

Fig. 4. Calcein-AM fluorescent images showing SH-SY5Y cultivated on top of the device for 24 h, 48 h and 168 h. (For interpretation of the references to color in this figure caption, the reader is referred to the web version of this article.)

To this purpose, SH-SY5Y cells were cultured in Dulbecco's Modified Eagle's Medium (DMEM) with 10% fetal bovine serum, 1% L-glutamine and 1% penicillin–streptomycin added. Cells were seeded in a Petri dish containing the PXC microelectrode with half of the active areas PEDOT-modified, as in the scheme in Fig. 1 – Supplementary Information. A 100 μl drop of culture medium containing 10,000 cells was deposited on the electrode surface and, after 4 h (the time required for cell adherence), 2 ml of culture medium was added, giving a cell concentration of 5000 cells/ml (see Fig. 5 – Supplementary Information). In this way, the cells were concentrated over the region of interest.

A viability assay was performed after 24 h, 72 h and 168 h using the LIVE/DEAD ® Viability/Cytotoxicity Assay Kit. The kit provides a two-color fluorescence cell viability assay that is based on the simultaneous determination of live and dead cells with two probes that measure recognized parameters of cell viability: intracellular esterase activity and plasma membrane integrity. The polyanionic dye calcein is well retained within live cells, producing an intense uniform green fluorescence in live cells. Ethidium homodimer-1 (EthD-1) enters cells with damaged membranes and undergoes a 40-fold enhancement of fluorescence upon binding to nucleic acids, thereby producing a bright red fluorescence in dead cells. EthD-1 is excluded by the intact plasma membrane of live cells. Fluorescence photos of SH-SY5Y cells cultured on PEDOT-modified PXC based microelectrodes are shown in Fig. 4. Cells appear to have spread homogeneously and to have proliferated quickly, demonstrating a good viability on our substrate.

3.6. *Cells morphology assessment*

The morphology of the cells on the electrode substrate was assessed through SEM. SH-SY5Y cells were seeded in a Petri dish as described above and cultured for 48 h and 168 h, then the fixation procedure was performed. Before proceeding to the SEM observation, the samples were sputtered with 10 nm of Au in order to avoid charging effect. Individual cells can be recognized in Fig. 6 – Supplementary Information. The cells display extensive processes and appear to be well attached on the surface of our electrodes. Importantly, they do not show a particular preference

for different materials and, as can be observed, they spread homogeneously both on PXC substrate and on PEDOT-modified electrode surface.

Neural recording and stimulating devices communicate with neurons via electrical signals (Richardson-Burns et al., 2007b), in particular, extracellular microelectrodes record the voltages produced by ionic current flow around neurons as their cell membranes depolarize as the result of inputs received from other cells. The attachment of cells on our electrode substrate shown in SEM images means that it is possible to get direct, long-term functional contact with the target tissue that is required to the implanted device to operate properly.

4. *In vivo* and *in vitro* signal recording

During an electrophysiological measurement, several noise sources, both biological and non-biological, can affect the recording. In particular, the non biological sources include the thermal noise, the electronic noise due to the amplifier, and the noise associated to the double layer interface (Baranauskas et al., 2011). Thermal noise is thought to be the dominant noise source encountered when performing cortical microelectrode recordings, it is directly related to the electrode impedance and as a consequence, it is also related to the surface area of the electrode contact (Lempka et al., 2006). This contribution to the noise can

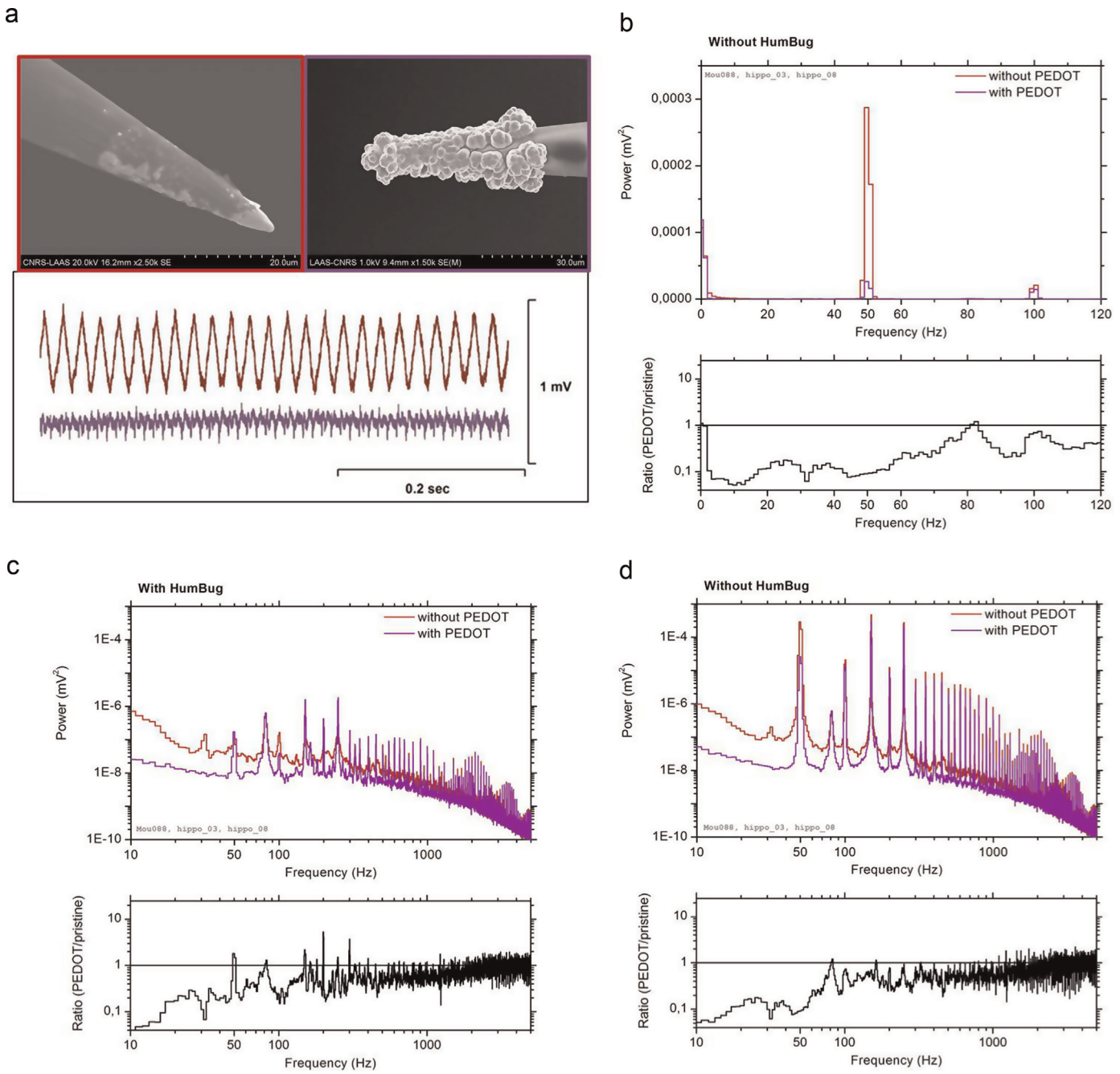

Fig. 5. (a) Comparison of electric hum recorded in a mouse brain slice maintained *in vitro*, using identical commercial microelectrodes: pristine (red) and nanostructured (violet). The signal was obtained by bypassing the HumBug, the device normally used to remove it. The 50 Hz hum is nearly negligible after nanostructuration. (b) The power spectra computed from a few seconds of the same recordings shows a prominent peak at 50 Hz when the recording was obtained with the non-nanostructured electrode. Noise power spectrum between 10 Hz and 5000 Hz (c) with and (d) without the HumBug, and related ratio of the power without/with PEDOT coating. (For interpretation of the references to color in this figure caption, the reader is referred to the web version of this article.)

Please cite this article as: Castagnola, V., et al., Biosensors and Bioelectronics (2014), http://dx.doi.org/10.1016/j.bios.2014.09.004

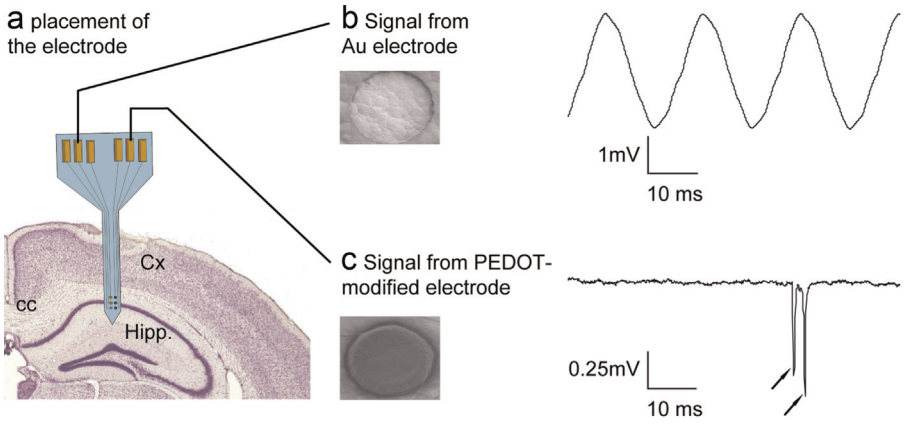

Fig. 6. (a) The hex-trode with 3 pristine electrodes and 3 PEDOT-modified electrodes was placed across the pyramidal layer of area CA1. Recordings were made from each electrode of the hex trode. (b) Electrophysiological signal obtained with a pristine gold electrode: note the prominent 50 Hz electromagnetic noise which completely occludes any biological signal. (c) Electrophysiological signal obtained with a PEDOT-modified electrode: note the two spontaneous extracellular action potentials (arrows) and the complete lack of 50 Hz noise. Cx: Cortex, cc: corpus collosum, Hipp.: hippocampus.

therefore be easily reduced by the increment in surface/area ratio given by PEDOT nanostructuration. Another effect of the PEDOT modification could be found in the removal of the electric hum at 50 Hz. The noise in signals obtained through commercially available microelectrodes (alphaOmega, FHC from the same batch, with identical characteristics), some of them used as received and the others coated with PEDOT, was evaluated. Fig. 5a shows that the unfiltered records obtained the same day and in the same experimental conditions (the same brain slice). Electric hum was considerable when recordings were performed through non-nanostructured electrodes, as shown on the red trace in Fig. 5a. In comparison, the hum was largely reduced with the nanostructured microelectrodes (violet curve in Fig. 5a). This is further quantitatively evidenced when examining the power spectra (Fig. 5b) computed from a few seconds of the same recordings. The prominent peak at 50 Hz observed for the non-modified microelectrode is hardly visible for the PEDOT-modified one. The same recording in the presence and absence of the HumBug line noise eliminator is shown in Fig. 5c and d. This comparison allows us to evaluate the noise component related to the double layer interface in the presence of PEDOT (Kozai et al., 2012). As we can see, also from the ratio of the power with and without PEDOT coating (lower part of the figure), the noise is reduced by PEDOT coating in both cases, especially at low frequencies, and, without the Humbug filter, the 50 Hz hum is reduced by a factor 10 through the PEDOT coating.

An additional validation of the PEDOT coating consisted in determining whether PEDOT coated microelectrodes allowed recording neuronal activity with a signal quality comparable to, or better than that achieved with non-coated electrodes. Fig. 7 – Supplementary Information shows action potentials recorded in area CA3 of the mouse hippocampus. The excellent signal-to-noise ratio of the PEDOT-modified microelectrode allowed us to obtain well segregated signals from three neighbouring neurons. This establishes that neuronal activity can be recorded with PEDOT coated microelectrodes with a quality at least comparable to that of non-coated microelectrodes. A quantitative comparison of single unit isolation quality with pristine and PEDOT-coated electrode is currently under-way.

The implantation of Parylene based electrodes in the brain of anaesthetized mice confirmed the improvement of the recording quality produced by PEDOT nanostructuration. As shown in Fig. 6b, the signal obtained with the pristine gold electrode is mainly composed of 50 Hz electromagnetic noise, with an amplitude comparable to that usually obtained before inserting the electrode in the brain or when the electrode is faulty. This is most likely a consequence of the small diameter of the electrode active area (20 μm), which resulted in a high impedance. On the opposite, lowering the impedance of the very same electrodes with PEDOT nanostructuration enabled the recording of very good electrophysiological signals with very high S.N.R. (Fig. 6c).

5. Conclusion

In conclusion, a simple fabrication protocol of implantable microelectrodes fully made of Parylene-C is reported. The cytotoxicity of the device has also been investigated *in vitro* after the fabrication procedure. We demonstrated that the electrochemical modification of the electrode active area with PEDOT greatly decreases the electrical impedance and our preliminary electrophysiological data suggest that PEDOT enhances the S.N.R. during *in vivo* and *in vitro* recording. This should allow a significant improvement of neurophysiological recordings quality. Signal recordings over several months are planned in the near future and will allow us to evaluate the electrical stability of our probes. The high biocompatibility of the proposed materials, the high degree of conformity provided by the soft substrate, the enhanced electrical properties and the stability of the PEDOT coating are an encouraging starting point for application in the field of medical diagnostic, treatment of several diseases and for the long-term implantation in disable patients. Signal recordings over several months are planned in the near future and will allow us to evaluate the electrical stability of our probes.

Acknowledgments

Part of this work was financially supported by the project NEUROSTIM from the University of Toulouse and the PIR-CNRS project NEURO-IC. This work was partly supported by the French RENATECH network.

Appendix A. Supplementary data

Supplementary data associated with this paper can be found in the online version at http://dx.doi.org/10.1016/j.bios.2014.09.004.

References

Abidian, M.R., Corey, J.M., Kipke, D.R., Martin, D.C., 2010. Small 6, 421–429.

Aregueta-Robles, U.A., Woolley, A.J., Poole-Warren, L.A., Lovell, N.H., Green, R.A., 2014. Front. Neuroeng. 7, 1–18.

Asplund, M., Thaning, E., Lundberg, J., Sandberg-Nordqvist, A.C., Kostyszyn, B., Inganäs, O., Holst, H.V., 2009. Biomed. Mater. 4, 045009.

Asplund, M., Nyberg, T., Inganas, O., 2010. Polym. Chem. 1, 1374–1391.

Baranauskas, G., Maggiolini, E., Castagnola, E., Ansaldo, A., Mazzoni, A., Angotzi, G.N., Vato, A., Ricci, D., Panzeri, S., Fadiga, L., 2011. J. Neural Eng. 8 (6), 066013.

Biran, R., Martin, D.C., Tresco, P.A., 2007. J. Biomed. Mater. Res.—Part A 82, 169–178.

Castagnola, V., Bayon, C., Descamps, E., Bergaud, C., 2014. Synth. Met. 189, 7–16.

Cui, X.T., Zhou, D.D., 2007. IEEE Trans. Neural Syst. Rehabil. Eng. 15, 502–508.

Cui, X., Lee, V.a., Raphael, Y., Wiler, J.a., Hetke, J.F., Anderson, D.J., Martin, D.C., 2001. J. Biomed. Mater. Res. 56, 261–272.

Edelman, E.R., Seifert, P., Groothuis, A., Morss, A., Bornstein, D., Rogers, C., 2001. Circulation 103, 429–434.

Gilletti, A., Muthuswamy, J., 2006. J. Neural Eng. 3, 189–195.

Griffith, R.W., Humphrey, D.R., 2006. Neurosci. Lett. 406, 81–86.

Harris, A.R., Morgan, S.J., Chen, J., Kapsa, R.M.I., Wallace, G.G., Paolini, A.G., 2013. J. Neural Eng. 10, 016004.

Hochberg, L.R., Serruya, M.D., Friehs, G.M., Mukand, J.A., Saleh, M., Caplan, A.H., Branner, A., Chen, D., Penn, R.D., Donoghue, J.P., 2006. Nature 442, 164–171.

Kim, B.J., Kuo, J.T.W., Hara, S.A., Lee, C.D., Yu, L., Gutierrez, C.A., Hoang, T.Q., Pikov, V., Meng, E., 2013. J. Neural Eng. 10, 045002.

Kim, Y.-T., Hitchcock, R.W., Bridge, M.J., Tresco, P.A., 2004. Biomaterials 25, 2229–2237.

Kipke, D.R., Shain, W., Buzsáki, G., Fetz, E., Henderson, J.M., Hetke, J.F., Schalk, G., 2008. J. Neurosci. 28, 11830–11838.

Kotov, N.A., Winter, J.O., Clements, I.P., Jan, E., Timko, B.P., Campidelli, S., Pathak, S., Mazzatenta, A., Lieber, C.M., Prato, M., Bellamkonda, R.V., Silva, G.a., Kam, N.W.S., Patolsky, F., Ballerini, L., 2009. Adv. Mater. 21, 3970–4004.

Kozai, T.D.Y., Langhals, N.B., Patel, P.R., Deng, X., Zhang, H., Smith, K.L., Lahann, J., Kotov, N.A., Kipke, D.R. 2012. Nat. Mater. 11, 1065–1073.

Lind, G., Linsmeier, C.E., Schouenborg, J., 2013. Scient. Rep. 3, 1–7.

Lempka, S., Johnson, M., Barnett, D., Moffitt, M., Otto, K., Kipke, D., McIntyre, C., 2006. In: 28th Annual International Conference of the IEEE Engineering in Medicine and Biology Society (EMBS'06), pp. 3361–3364.

Metallo, C., White, R.D., Trimmer, B.A., 2011. J. Neurosci. Methods 195, 176–184.

Nowak, L., Bullier, J., 1996. J. Neurosci. Methods 67, 237–248.

Polikov, V.S., Tresco, P.a., Reichert, W.M., 2005. J. Neurosci. Methods 148, 1–18.

Polikov, V.S., Block, M.L., Fellous, J.-M., Hong, J.-S., Reichert, W.M., 2006. Biomaterials 27, 5368–5376.

Richardson-Burns, S.M., Hendricks, J.L., Foster, B., Povlich, L.K., Kim, D.-H., Martin, D.C., 2007a. Biomaterials 28, 1539–1552.

Richardson-Burns, S.M., Hendricks, J.L., Martin, D.C., 2007b. J. Neural Eng. 4, L6–L13.

Rodger, D.C., Fong, A.J., Li, W., Ameri, H., Ahuja, A.K., Gutierrez, C., Lavrov, I., Zhong, H., Menon, P.R., Meng, E., Burdick, J.W., Roy, R.R., Edgerton, V.R., Weiland, J.D., Humayun, M.S., Tai, Y.-C., 2008. Sens. Actuators B: Chem. 132, 449–460.

Rousche, P.J., Normann, R.A., 1998. J. Neurosci. Methods 82, 1–15.

Sankar, V., Sanchez, J.C., McCumiskey, E., Brown, N., Taylor, C.R., Ehlert, G.J., Sodano, H.a., Nishida, T., 2013. Front. Neurol. 4, 1–11.

Schwartz, A.B., Cui, X.T., Weber, D.J., Moran, D.W., 2006. Neuron 52, 205–220.

Sekli-Belaidi, F., Temple-Boyer, P., Gros, P., 2010. J. Electroanal. Chem. 647, 159–168.

Seymour, J., Langhals, N., Anderson, D., Kipke, D., 2011. Biomed. Microdev. 13, 441–451.

Streit, B.W.J., Sankar, V., Knott, E., Dyer, A., Reynolds, J.R., Nishida, T., Shaw, G.P., Sanchez, J.C., 2012. IEEE Pulse. 3, 30–33.

Xiao, Y., Martin, D.C., Cui, X., Shenai, M., 2006. Appl. Biochem. Biotechnol. 128, 117–129.

Yamato, H., Ohwa, M., Wernet, W., 1995. J. Electroanal. Chem. 397, 163–170.

Ziegler, D., Suzuki, T., Takeuchi, S., 2006. J. Microelectromech. Syst. 15, 1477–1482.

Zitter, H., Plenk, H., 1987. J. Biomed. Mater. Res. 21, 881–896.

Please cite this article as: Castagnola, V., et al., Biosensors and Bioelectronics (2014), http://dx.doi.org/10.1016/j.bios.2014.09.004